RSC Advances

ROYAL SOCIETY OF CHEMISTRY

www.rsc.org/advances

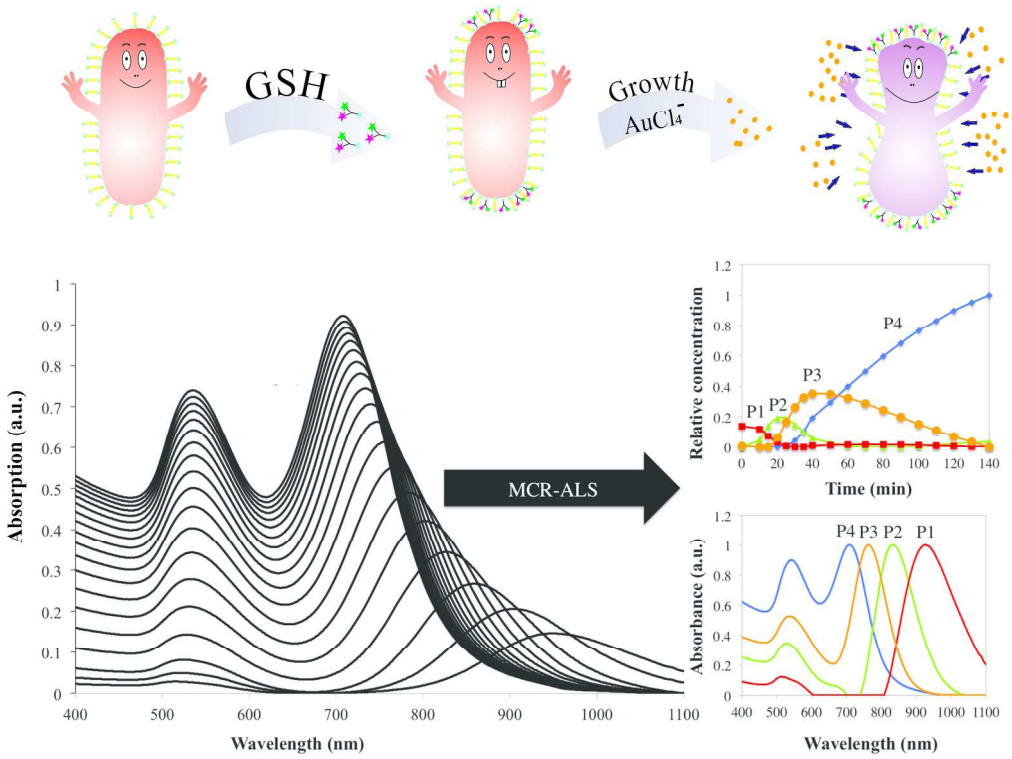

217x163mm (300 x 300 DPI)

Colorimetric Detection of Glutathione Based on Transverse Overgrowth of High Aspect Ratio Gold Nanorods Investigated by MCR-ALS

Nafiseh Fahimi-Kashani, [†] *Parisa Shadabipour, and* [†] *M. Reza Hormozi Nezhad* *[,†,‡]

[†]*Department of Chemistry, Sharif University of Technology, Tehran 11155-9516, Iran*

[‡]*Institute of nanoscience and nanotechnology, Sharif University of Technology, Tehran, Iran*

KEYWORDS: Gold nanorods (GNRs), Glutathione (GSH), colorimetric detection, MCR-ALS

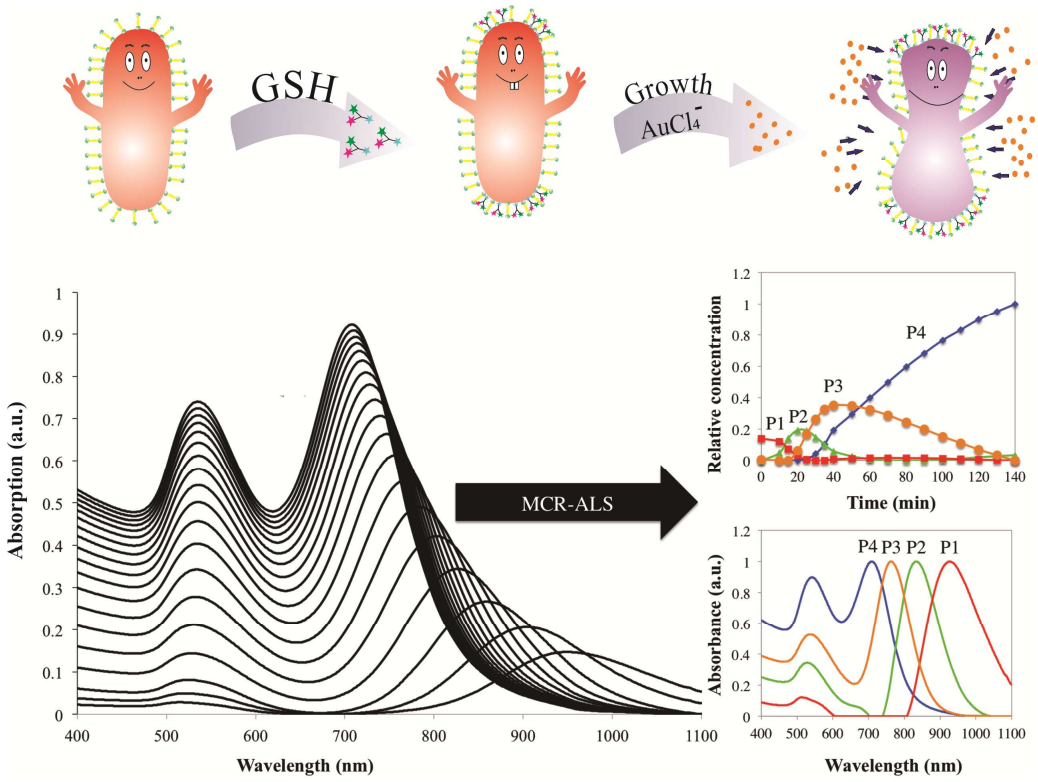

Abstract

In this paper, we present a simple platform for colorimetric detection of glutathione using gold nanorods (AR ~ 6.5 ± 0.2) as a plasmonic sensor. The functional mechanism of the sensor is based on shifts of longitudinal plasmon resonance during selective transverse overgrowth induced by preferential binding of glutathione at nanorods tips. Under the optimum condition, calibration curve showed two linear regimes at the range of 50 nM to 20 μM of glutathione with detection limit as low as 40 nM. The nanosensor maintains relatively high selectivity for determination of glutathione in presence of several other amino acids. However, cysteine at similar concentration level strongly competes with glutathione for available binding sites, thereby interfering in determination of glutathione. We employed Multivariate curve resolution-alternating least square (MCR-ALS) to track morphology variation of nanorods and elucidate the kinetic of overgrowth process in presence of glutathione and cysteine.

1. Introduction

Recent years have seen renewed interest for developing methods in the quest for determination of thiol-containing molecules in biological matrix [1]. Glutathione (GSH), a tripeptide (γ-L-glutamyl-L-cysteinyl-glycine), is the most abundant cytosolic thiol in mammalian tissues and fluids with concentration that covers several orders of magnitude, from nM in condensate exhaled breath to μM in saliva, serum and urine, and typical concentration of mM in whole blood [2]. Similar to other biological thiols, GSH serves many vital biological functions in human pathologies, such as regulating cellular redox activities and preventing cell damage through scavenging free radical and peroxides [3-5]. The overall cells health is related to the ratio of reduced form of glutathione (GSH) to its oxidized form (GSSG) for which a value of more than nine is an indication of healthy living cells [6]. However, pathological conditions such as oxidative stress can cause conversion of GSH to GSSG, thus negatively affect the ratio of GSH to GSSG. On the other hand, abnormal intracellular level of reduced GSH are associated with various diseases, such as Parkinson, Alzheimer, human immunodeficiency virus (HIV), liver damage, cardio- vascular diseases (CVDs), etc [7-11]. Hence, monitoring and determination of GSH level is of great importance for assessing cell functions and early diagnosis of clinical disorder. Up to now, several techniques, such as electroanalytical methods [12, 13], florescence [14-17], chemiluminescence [18, 19], hyphenated techniques [20, 21], Raman spectroscopy [22, 23], spectrophotometry [24], and capillary electrophoresis [25, 26] have been developed and proven to be promising for sensitive and selective determination of glutathione with detection limit improved to some extent. However, the attachment between specialized instrumentation, expensive reagents, and tedious and taxing sample preparation procedure implores novel technique for simple, cost-effective, and fast, yet sensitive measurements for practical applications.

The past two decades has witnessed considerable contribution for developing Localized surface plasmon resonance (LSPR) sensors as a simple and powerful tool for chemical and biological sensing [27-30]. This is fueled by fascinating optoelectrical properties of plasmonic nanomaterials that offers unique features for chemical and biological sensing that are not accessible with conventional analytical methods [31-37]. In this context, gold nanorods (Au NRs) have been receiving extensive attention, in large part owing to their strong extinction coefficient at longitudinal surface plasmon (LSP) resonance, which is dependent on their size, aspect ratio (AR) and refractive index of surrounding media [38, 39]. Since the first report on synthesis of rodlike Au nanoparticles almost two decades ago [40, 41], there have been great strides both in terms of improving synthetic protocols and tunning their surface plasmon resonance [42-49] as well as their implementation as building block of plasmonic nanosensors [39, 50-57]. Those achievements have led to significant advances in science and technology of LSPR sensors.

In this paper, we presented a simple colorimetric method for determination of very low quantities of glutathione in complex solution. Here, our study is inspired by previous report on transverse overgrowth of Au NRs induced by preferential binding of glutathione at nanorods tips [58]. Au NRs with aspect ratio as long as 6.5 ± 0.2 and corresponding LSP of around 940nm was synthesized and utilized as a plasmonic sensor. Long aspect ratio of NRs enabled us to more precisely track the variations of LSP in low quantity of glutathione. Under optimized condition, glutathione was detected with detection limit down to nM. In addition, we coupled multivariate curve resolution-alternating least square (MCR-ALS) technique to UV/Vis absorption spectroscopy measurements to monitor morphology changes of NRs during transverse overgrowth process. As it will be demonstrated in this article, the obtained MCR-ALS results faithfully corroborates the TEM results of previous study [58]. Finally, MCR-ALS analysis was

successfully employed to elucidate the kinetic of transverse overgrowth on Au NRs induced by cysteine and its comparison with glutathione.

2. Experimental and methods

2.1. Reagents

Hydrogen tetrachloroaurate ($HAuCl_3.3H_2O$), Silver nitrate ($AgNO_3$), sodium borohydride ($NaBH_4$), cetyltrimethylammonium bromide (CTAB), 5-Bromosalicylic acid (5-Br-SA), ascorbic acid (AA), sodium hydroxide (NaOH), Hydrochloric acid (HCl), and Glutathione (GSH) was purchased from Merck and were used without further purification.

2.2. Apparatus

Extinction spectra were recorded using a PerkinElmer (Lambda25) spectrophotometer with a 1.0 cm glass cell. Measurements of pH were performed with a Denver Instrument Model of 270 pH meter equipped with a Metrohm glass electrode. Transmission electron microscopy (TEM) images were recorded with a PHILIPS MC 10 TH microscope (USA) at an accelerating voltage of 100 kV. Water used for preparation of all samples, was purified with cartridges from Millipore (Milli-Q) to a resistively of 18.2 MΩ.

2.3. Preparation of high aspect ratio Au NRs

A stock solution of Au NRs were prepared in accordance with the existing procedure with minor modification [59]. Briefly, seed solution was prepared by mixing 5.0 mL of 0.1 M CTAB with 0.05 mL solution of 2.5×10^{-2} M $HAuCl_4$ followed by injection of 0.3 mL of 0.01 M ice-cold $NaBH_4$ to this solution under vigorous stirring. The resulted brownish yellow solution was stirred for 3 min and left at room temperature for about 2hr before utilizing for the next step. For preparation

of the growth solution, 0.015 gr 5-Br-SA was added to 50 mL of 0.05M CTAB under gentle stirring. This was followed by addition of 1.15 mL of 0.01 M $AgNO_3$. The mixture was kept undisturbed for 15 min, then 1mL of 2.5×10^{-2} M $HAuCl_4$, 0.40 mL of HCl (37 wt % in water, 12.1 M) and 0.30 mL of 0.10 M ascorbic acid were added one by one. Finally 0.06 mL of CTAB-capped gold seeds was injected into the solution under gentle stirring. The color of solution gradually changed within 1hr, and the solution left undisturbed overnight at ambient temperature of 27°C to complete growth process.

2.4. Determination of glutathione and calibration curve

Determination of glutathione was accomplished on the basis of selective transverse overgrowth of original nanorods from addition of growth solution to aliquot of original nanorods in presence of glutathione. For this purpose, a growth solution was prepared according to previous section, except that seed solution was not added. Several experiments were carried out to optimize the volume of growth solution, time of overgrowth process, and pH. Under optimized condition, different concentrations of glutathione were added to the 1 ml of aliquot of nanorods (5 pM), and the solution mixture incubated for 15 min. This was followed by addition of growth solution and adjusting the final volume to 3.6 ml. The UV-Vis spectra of the solutions were recorded at room temperature at t=0 min and t=60 min. Here, the difference between surface area of the extinction spectrum in absence and presence of growth solution at the range of 650 nm to 1100 nm was chosen as a response.

2.5. Preparation of human plasma sample

1.5 mL of 10% Trichloroacetic acid solution was added to the freshly human plasma sample and mixed well to precipitate proteins. After centrifuging at 8000 rpm for 15 min,

the supernatant was removed and diluted 20-fold and succeeding analysis was carried out under the optimized conditions [85].

2.6. MCR-ALS analysis

The well-established soft-modeling methods of MCR-ALS is applied to decompose bilinear data matrix of recorded spectra into sub-matrices of **C**(r×n) and **S**(n×c) that represent the concentration profile and pure spectra of involved absorbing components (n), respectively. Here, the recorded evolutionary absorbance spectra from addition of growth solution to NRs-GSH system was considered as a data matrix D(r×c), where r equals to 18 and corresponds to number of recorder spectra and c equals to 701 and referred to the number of monitored wavelengths in the range of 1100 nm-400 nm (with 1.0 nm intervals). Statistical and chemometrics analysis were performed in MATLAB (Mathwork, Inc., R2014a, 8.3) environment. The subroutine for MCR-ALS analysis was downloaded from latest version of MCR-ALS GUI 2.0 developed by Jaumot et al. [60]. This version of MCR-ALS is capable of performing all required statistical analysis for MCR-ALS outset including principal component analysis using singular value decomposition (SVD) algorithm for evaluating number of components possessing distinguished spectral characteristics and evolving factor analysis (EFA) for obtaining initial concentration of profile of the detected species as a function of reaction time. Iterative algorithm of ALS was performed on varied number of components with aim to minimize the lack of fit (LOF) of MCR–ALS model in the error matrix **E** [61].

3. Result and discussion

3.1. Glutathione-induced transverse overgrowth on Au nanords

Figure 1 shows normalized extinction spectra and TEM images of the Au NRs before and after transverse overgrowth induced by 5 μM of Glutathione. The original nanorods exhibit narrow

size distribution (Fig. 1b) with an average aspect ratio of 6.5 ± 0.2 (length of 65 ± 6 nm and width of 10 ± 2 nm). The extinction spectrum of as-prepared nanorods in figure 1a shows a relatively sharp longitudinal surface plasmon resonance (LSPR) at 940nm without any shoulder or extra peak from impurities. The LSP maxima is in agreement with linear fit to the experimentally determined NRs aspect ratio by Ye et al. [59]. Concentration of nanorods was estimated to be ~ 0.05 nM according to previously measured aspect ratio-dependent extinction coefficient for nanorods [62]. As can be seen in figure 1a, the overgrowth on pristine NRs in presence glutathione causes a blue shift on LSPR extinction along with increasing the intensity of plasmon maxima (see figure 2). Upon completing the growth process, the corresponding TEM image of NRs shows an increase in width while their length are relatively remained unchanged (Fig. 1c). End-to-end self-assembly of Au NRs in presence of thiol containing linkers has been well known since early reports on Au NRs synthesis [63-66]. This phenomenon is governed by preferential bounding of thiol functional group to the NRs tip for that different mechanisms there exists [63, 65-67]. Such a preferential binding was recently exploited to open a pathway for selective transverse overgrowth on NRs (scheme 1) [58]. Herein, we assessed the effects of different parameters on overgrowth process with aim to develop a simple colorimetric sensor for detection of glutathione in complex system.

3.2. Effect of growth solution volume/overgrowth reaction time

Figure 2 (a-f) shows the variation of UV-Vis spectra of Au NRs during glutathione (5 μM)-induced transverse overgrowth from addition of different volume of growth solution. All spectra of the growth products were recorded within 150 min with 10 min intervals. As the reaction is preceded a clear blue shift in LSP is observed that reflects morphology changes accompanied by reduction in aspect ratio of NRs. A few nm red shift of transverse plasmon frequency is

discernable at higher volume of growth solution that indicates formation of wider nanorods. In addition, the intensity ratio of transverse to longitudinal maxima is proportional to the amount of Au precursor in final solution as the volume of growth increases. The overall overgrowth process is directly related to the volume of growth solution, as blue shift of LSP is more significant at higher volume of growth solution. However, increasing the volume of growth solution to more than 1.5 mL did not have significant influence on LSP shift and surface area at the range of 650 nm to 1100 nm (Fig. 2i). Furthermore, increasing the volume of growth solution was accompanied by increasing the time required for completing overgrowth process (Fig. 2h). From these observations, we opted the volume of growth solution and reaction time to be 1.5 mL and 60 min, respectively, for determination of glutathione.

3.3. Effect of pH

Controlling the pH seems to be critical for overgrowth process as longitudinal growth on Au NRs is impeded due to binding of GSH molecules through their zwitterionic groups [56]. In order to control the pH of final solution the pH of original nanorods were adjusted in broad range from 2.29 to 9.32 for that NRs showed very good stability (Fig. S1). However, it was found that pH of original NRs does not significantly contribute to the pH of final solution. In fact, the pH of final solution generally stays at the range of 1.6-1.8 because of acidic nature of growth solution used for overgrowth process (Fig. S2). In addition, efforts for adjusting pH of growth solution remained unfulfilled as increasing pH of growth solution led to formation of nanoparticles with plasmon resonance appeared at around 520 nm (Fig. S3). According to the dissociation constants of GSH, this molecule exists in zwitterionic form at pH~1.6-1.8. Hence, determination of glutathione was conducted at natural pH of final solution.

3.4 Determination of glutathione

3.4.1 Calibration curve

Figure 3, shows the results for colorimetric determination of GSH based on transverse overgrowth on Au NRs induced by varying concentration of GSH under optimum condition. As can be seen, increasing concentration of GSH is associated with noticeable blue shift for LSP, at constant volume of growth solution, as longitudinal growth is more effectively prevented at higher concentration of GSH. The transverse overgrowth can be further evidenced by an increase in intensity of transverse peak along with 30 nm red shift as the concentration of GSH increases to 20 μM. According to the previous study, at certain concentration of GSH both longitudinal and transverse growths are blocked due to linear assembly of original NRs that consequently results in red shift in LSP [66]. Obviously such a critical concentration of GSH depends on parameters such as concentration and dimensions of original NRs, and the amount of gold precursor in growth solution. In the present case, the red shift of LSP was experimentally started at GSH concentration as low as 20 μM because the present system utilized low concentration of reagents in order to improve the detection limit for determine of GSH. The calculated calibration curve in Fig 3c revealed two linear regimes at concentration ranges of 50 nM-1 μM and 1 μM-20 μM. The calculated limit of detection (LOD) and limit of quantification (LOQ) were 40 nM and 130 nM, respectively. The standard deviation was also calculated at linear regime based on five measurements for different concentrations of GSH, including 15, 8, 1.5, 0.25, and 0.05 μM. The obtained RSDs% were 1.9-4.7 and 1.2-4.7 at concentration range of 50 nM-1 μM and 1 μM-20 μM, respectively.

3.4.2 Real sample analysis and Interferences study

To assess the ability of the proposed method for the determination of glutathione in complex samples, the interference of nine foreign amino acids were evaluated on selectivity of the method. This was conducted through overgrowth of NRs in presence of 10 μM glutathione compared with overgrowth process in presence of other amino acids with concentration 50 times higher. Among tested amino acids, Methionine, Alanine, Lysine, and Glycine, did not interfere, while Tryptophan, Tyrosine, Proline and Phenylalanine showed some interference (Figure 4). The optimized method was applied for the determination of glutathione in complex sample containing low concentration of glutathione and nine co-existing amino acids. Likewise, the proposed method was used to detect GSH in human plasma sample and the results were compared with the results obtained by a standard HPLC method [85]. The results, are given in Table 1, indicate the potential and feasibility of the developed method for simple and fast determination of glutathione in complex samples. A comparison between present method and conventional methods for detection of GSH is provided in Table 2. The obtained sensitivity of the present methods for colorimetric determination of GSH in standards is on a par with conventional techniques albeit without the use of probe molecule or labeling, and employing sophisticated instrumentation. Moreover, the obtained detection limit, recovery percentage and reproducibility of present method for determination of GSH in complex analyte mixture containing other aminothiols (except cysteine) is comparable to the literature.

3.5. MCR-ALS analysis

Spectroscopic methods are providing simple and low-cost complement to well-established sophisticated TEM technique for morphology characterization of nanomaterials. In particular,

when the spectroscopic data are coupled to multivariate curve resolution analysis it would be possible to decrypt useful information about the morphology variation as well as kinetic of process [68-75]. We employed MCR-ALS analysis to investigate the presence of intermediate nanorods species with distinct morphology and spectral characteristics during glutathione-induced transverse overgrowth on Au NRs. Our analysis considered the recorded evolutionary absorption spectra in figure 2d (1.5 mL growth solution, 5 μM glutathione) as a column-wise arranged data matrix D(18×701). The MCR-ALS analysis was performed on the data matrix considering four coexisting chemical component as suggested by SVD and EFA analyses. At convergence, the resulting lack of fit (LOF) error for root mean square of the differences between the absorbances calculated by the MCR-ALS model and those obtained experimentally was 1.75. Also, the lack of fit (LOF) error for root mean square of the differences between the absorbances calculated by the MCR-ALS model those reproduced by FA was 0.47. The calculated LOF errors were very low for that the resulting MCR-ALS model could reproduce 99.97% of variances in the experimental data. Figure 5 presents the normalized optimum concentration and resolved pure spectral profiles of the detected components calculated by MCR-ALS. The original nanorods exhibit a LSP at 940 nm and its concentration in the solution starts to diminish right after addition of growth solution. This is accompanied by evolving a new component (P2) with lower aspect ratio as evidenced by more than 100nm blue shift at LSP. The concentration of original nanorods drops to zero after 20min later that convincingly matches with maximum concentration of the component P2. This is followed by a decrease in concentration of P2 as it starts converting to component P3, which apparently has a lower aspect ratio with its corresponding blue shift in resolved pure spectral profile. Finally, as the component P3 is heading toward maximum concentration, the final component (P4) start to evolve and its

concentration reaches maximum at the end of reaction in which the concentration of all other structures is negligible. This component has a LSP at around 700nm that according to our TEM results and also finding of X. Kou et al. [58] by TEM imaging can be assigned to the peanut-shaped nanoparticles. Hence, species of P2, and P3, which were not characterized in the past, can be assigned to particles with evolving morphology between NRs and peanut-shaped nanoparticles. Since the system under study was optimized for detection of low quantities of glutathione, only low volume of growth solution and low concentration of GSH was utilized that were not capable of converting original nanorods to ultimate faceted spheres with single plasmon maxima characteristic [58]. SVD and EFA analysis were also performed for systems containing other volumes of growth solution, and interestingly four factors were suggested in all cases. The calculated optimum concentration profiles of the resolved particles represented similar trend to figure 5a with nominal LOF errors (Fig. S4-S5). It should be noted that NRs utilized in this article had longer aspect ratio in compare to previous work, and therefore the resolved concentration profiles and pure spectra of the detected species might be considered hypothetical unless they are confirmed by experimental determination of the individual species.

3.6. Investigation of kinetic of cysteine-induced transverse overgrowth on Au nanorods

Cysteine with the similar concentration of glutathione can induce overgrowth process [58], thereby strongly interferes during determination of glutathione. To gain more insight into kinetic of cysteine-induced transverse overgrowth on Au NRs, we investigated the transverse overgrowth on Au NRs in solutions possessing three different concentrations of cysteine and glutathione (Figure 6a-c). Interestingly, different kinetic of overgrowth process was observed in presence of cysteine than that of glutathione and their absence. The difference is becoming more pronounced at higher concentrations. As can be seen, for all different concentrations, variation of surface area

at the range of 650 nm to 1100 nm is more significant compare to overgrowth process induced by glutathione. To supports this observation, MCR-ALS was undertaken to analysis the recorded extinction spectra during overgrowth process induced by 5 μM micro of cysteine and the results are given in figure 6 d,e. Here, four chemical components with distinguished spectral features and concentration profiles were detected, similar to those calculated for glutathione-induced overgrowth process. However, the kinetic of overgrowth process on Au NRs in presence of cysteine is vividly faster as the relative concentration of component P1 (original nanorods) much faster drops to zero along with sharp rise in concentration of component P4 at early stages of reaction (see figure 5a for comparison). The final product (P4) exhibits a LSP at around 700 nm similar to those obtained in the case of glutathione (see figure 5b). This implies that the overall performance of glutathione and cysteine, at same concentration level, is similar for inducing overgrowth process, yet presenting different kinetics.

4. Conclusion

In summary, Au NRs with aspect ratio of 6.5 ± 0.2 were utilized as a simple plasmonic sensor for colorimetric determination of glutathione based on resonance shift of longitudinal plasmon while undergoing selective transverse overgrowth of nanorods induced by preferential binding of probe molecule at nanorods tips. This nanosensor maintains high selectivity for determination of glutathione in complex system containing several other amino acids, except of cysteine. Under optimized condition, the plotted calibration curve in a range of 50 nM to 20 μM showed good linearity, acceptable accuracy, and reproducibility with quantification limit as low as 130 nM was achieved. Moreover, MCR-ALS analysis was undertaken to resolve concentration and pure spectral profiles of intermediate species to gain better understanding of kinetic of transverse overgrowth in presence of glutathione and cysteine. Our finding can provide an impetus of

design and developing a colorimetric sensor for simultaneous determination of glutathione and cysteine.

ACKNOWLEDGMENT

The authors wish to express their gratitude to Sharif University of Technology Research Council for the support of this work.

Corresponding Author

* Email: hormozi@sharif.edu

References

1. H. S. Jung, X. Chen, J. S. Kim and J. Yoon, *Chemical Society Reviews*, 2013, **42**, 6019-6031.
2. A. Pastore, G. Federici, E. Bertini and F. Piemonte, *Clinica Chimica Acta*, 2003, **333**, 19-39.
3. V. Seth, B. D. Banerjee and A. K. Chakravorty, *Pesticide Biochemistry and Physiology*, 2001, **71**, 133-139.
4. A. Galano and J. R. Alvarez-Idaboy, *RSC Advances*, 2011, **1**, 1763-1771.
5. E. Sivan, Lee, Y.-C., Wu, Y.-K. and Reece, E. A., *Teratology*, 1997, **56**, 343-349.
6. M. Asensi, J. Sastre, F. V. Pallardo, A. Lloret, M. Lehner, J. Garcia-de-la Asuncion and J. Viña, in *Methods in Enzymology*, ed. P. Lester, Academic Press, Editon edn., 1999, vol. Volume 299, pp. 267-276.
7. S. M. K. Nazzareno Ballatori, Sylvia Notenboom, Shujie Shi, Kim Tieu, Christine L. Hammond, *Biological Chemistry*, 2009, **390**, 191-214.
8. V. Cavalca, Veglia, F., Squellerio, I., Marenzi, G., Minardi, F., De Metrio, M., Cighetti, G., Boccotti, L., Ravagnani, P. and Tremoli, E., *European Journal of Clinical Investigation*, 2009, **39**, 267-272.
9. D. M. Townsend, K. D. Tew and H. Tapiero, *Biomedicine & Pharmacotherapy*, 2003, **57**, 145-155.
10. L. A. Herzenberg, S. C. De Rosa, J. G. Dubs, M. Roederer, M. T. Anderson, S. W. Ela, S. C. Deresinski and L. A. Herzenberg, *Proceedings of the National Academy of Sciences of the United States of America*, 1997, **94**, 1967-1972.
11. R. a. N. Njälsson, S., *Acta Paediatrica,* , 2005, **94**, 132-137.
12. J. C. Harfield, C. Batchelor-McAuley and R. G. Compton, *Analyst*, 2012, **137**, 2285-2296.
13. M. K. Sezgintürk and E. Dinçkaya, *Biosensors and Bioelectronics*, 2004, **19**, 835-841.
14. H.-H. Cai, H. Wang, J. Wang, W. Wei, P.-H. Yang and J. Cai, *Dyes and Pigments*, 2012, **92**, 778-782.
15. X. Hou, X. Guo, B. Chen, C. Liu, F. Gao, J. Zhao and J. Wang, *Sensors and Actuators B: Chemical*, 2015, **209**, 838-845.
16. M. Hao, R. Liu, H. Zhang, Y. Li and M. Jing, *Spectrochimica Acta Part A: Molecular and Biomolecular Spectroscopy*, 2014, **125**, 7-11.
17. X. Tan, Y. Du, B. Yang and C. Ma, *RSC Advances*, 2015, **5**, 55165-55169.
18. H.-Y. Han, Z.-K. He and Y.-E. Zeng, *Microchimica Acta*, 2006, **155**, 431-434.
19. S. Wang, H. Ma, J. Li, X. Chen, Z. Bao and S. Sun, *Talanta*, 2006, **70**, 518-521.
20. I. Squellerio, D. Caruso, B. Porro, F. Veglia, E. Tremoli and V. Cavalca, *Journal of Pharmaceutical and Biomedical Analysis*, 2012, **71**, 111-118.
21. A. K. Sakhi, R. Blomhoff and T. E. Gundersen, *Journal of Chromatography A*, 2007, **1142**, 178-184.
22. L. Ouyang, L. Zhu, J. Jiang and H. Tang, *Analytica Chimica Acta*, 2014, **816**, 41-49.
23. G. G. Huang, X. X. Han, M. K. Hossain and Y. Ozaki, *Analytical Chemistry*, 2009, **81**, 5881-5888.
24. S.-C. Liang, H. Wang, Z.-M. Zhang, X. Zhang and H.-S. Zhang, *Analytica Chimica Acta*, 2002, **451**, 211-219.
25. J. Hodáková, J. Preisler, F. Foret and P. Kubáň, *Journal of Chromatography A*, 2015, **1391**, 102-108.
26. K. Govindaraju, V. Govindaraju and D. H. Eidelman, *Journal of Chromatography B*, 2003, **788**, 369-376.
27. K. M. Mayer and J. H. Hafner, *Chemical Reviews*, 2011, **111**, 3828-3857.
28. E. Kazuma and T. Tatsuma, *Nanoscale*, 2014, **6**, 2397-2405.
29. K. A. Willets and R. P. Van Duyne, *Annual Review of Physical Chemistry*, 2007, **58**, 267-297.

30. J. N. Anker, W. P. Hall, O. Lyandres, N. C. Shah, J. Zhao and R. P. Van Duyne, *Nat Mater*, 2008, **7**, 442-453.
31. M. B. Cortie and A. M. McDonagh, *Chemical Reviews*, 2011, **111**, 3713-3735.
32. P. D. Howes, S. Rana and M. M. Stevens, *Chemical Society Reviews*, 2014, **43**, 3835-3853.
33. M. Hu, J. Chen, Z.-Y. Li, L. Au, G. V. Hartland, X. Li, M. Marquez and Y. Xia, *Chemical Society Reviews*, 2006, **35**, 1084-1094.
34. T.-D. Nguyen and T.-H. Tran, *RSC Advances*, 2014, **4**, 916-942.
35. N. C. Lindquist, M. A. Turner and B. P. Heppner, *RSC Advances*, 2014, **4**, 15115-15121.
36. Y. Leng, K. Xie, L. Ye, G. Li, Z. Lu and J. He, *Talanta*, 2015, **139**, 89-95.
37. Y. Leng, Y. Li, A. Gong, Z. Shen, L. Chen and A. Wu, *Langmuir*, 2013, **29**, 7591-7599.
38. H. Chen, L. Shao, Q. Li and J. Wang, *Chemical Society Reviews*, 2013, **42**, 2679-2724.
39. J. Cao, T. Sun and K. T. V. Grattan, *Sensors and Actuators B: Chemical*, 2014, **195**, 332-351.
40. C. A. Foss, G. L. Hornyak, J. A. Stockert and C. R. Martin, *The Journal of Physical Chemistry*, 1992, **96**, 7497-7499.
41. C. A. Foss, G. L. Hornyak, J. A. Stockert and C. R. Martin, *The Journal of Physical Chemistry*, 1994, **98**, 2963-2971.
42. B. Nikoobakht and M. A. El-Sayed, *Chemistry of Materials*, 2003, **15**, 1957-1962.
43. S. E. Lohse and C. J. Murphy, *Chemistry of Materials*, 2013, **25**, 1250-1261.
44. T. K. Sau and C. J. Murphy, *Langmuir*, 2004, **20**, 6414-6420.
45. A. Gole and C. J. Murphy, *Chemistry of Materials*, 2004, **16**, 3633-3640.
46. A. M. Alkilany, L. B. Thompson and C. J. Murphy, *ACS Applied Materials & Interfaces*, 2010, **2**, 3417-3421.
47. M. Reza Hormozi-Nezhad, H. Robatjazi and M. Jalali-Heravi, *Analytica Chimica Acta*, 2013, **779**, 14-21.
48. J. Pérez-Juste, I. Pastoriza-Santos, L. M. Liz-Marzán and P. Mulvaney, *Coordination Chemistry Reviews*, 2005, **249**, 1870-1901.
49. J. Pérez-Juste, Liz-Marzán, L. M., Carnie, S., Chan, D. Y. C. and Mulvaney, P., *Adv. Funct. Mater.*, 2004, **14**, 571-579.
50. L. P. K. Vigderman, Bishnu, and R. Zubarev Eugene *Adv. Mater.*, 2012, **24**, 4811-4841.
51. E. Yasun, H. Kang, H. Erdal, S. Cansiz, I. Ocsoy, Y.-F. Huang and W. Tan, *Interface Focus*, 2013, **3**, 20130006.
52. M. A. Mahmoud and M. A. El-Sayed, *The Journal of Physical Chemistry Letters*, 2013, **4**, 1541-1545.
53. C. H. Lee, L. Tian and S. Singamaneni, *ACS Applied Materials & Interfaces*, 2010, **2**, 3429-3435.
54. B. Saute, R. Premasiri, L. Ziegler and R. Narayanan, *Analyst*, 2012, **137**, 5082-5087.
55. Y. Zhu, H. Kuang, L. Xu, W. Ma, C. Peng, Y. Hua, L. Wang and C. Xu, *Journal of Materials Chemistry*, 2012, **22**, 2387-2391.
56. G. Lu, L. Hou, T. Zhang, J. Liu, H. Shen, C. Luo and Q. Gong, *The Journal of Physical Chemistry C*, 2012, **116**, 25509-25516.
57. R. A. Alvarez-Puebla, A. Agarwal, P. Manna, B. P. Khanal, P. Aldeanueva-Potel, E. Carbó-Argibay, N. Pazos-Pérez, L. Vigderman, E. R. Zubarev, N. A. Kotov and L. M. Liz-Marzán, *Proceedings of the National Academy of Sciences*, 2011, **108**, 8157-8161.
58. X. Kou, S. Zhang, Z. Yang, C.-K. Tsung, G. D. Stucky, L. Sun, J. Wang and C. Yan, *Journal of the American Chemical Society*, 2007, **129**, 6402-6404.
59. X. Ye, L. Jin, H. Caglayan, J. Chen, G. Xing, C. Zheng, V. Doan-Nguyen, Y. Kang, N. Engheta, C. R. Kagan and C. B. Murray, *ACS Nano*, 2012, **6**, 2804-2817.
60. J. Jaumot, A. de Juan and R. Tauler, *Chemometrics and Intelligent Laboratory Systems*, 2015, **140**, 1-12.
61. A. de Juan, M. Maeder, M. Martínez and R. Tauler, *Chemometrics and Intelligent Laboratory Systems*, 2000, **54**, 123-141.

62. R. D. Near, S. C. Hayden, R. E. Hunter, D. Thackston and M. A. El-Sayed, *The Journal of Physical Chemistry C*, 2013, **117**, 23950-23955.
63. K. K. Caswell, J. N. Wilson, U. H. F. Bunz and C. J. Murphy, *Journal of the American Chemical Society*, 2003, **125**, 13914-13915.
64. A.-q. Yang, D. Wang, X. Wang, Y. Han, X.-b. Ke, H.-j. Wang, X. Zhou and L. Ren, *RSC Advances*, 2015, **5**, 38354-38360.
65. Y. Wang, A. E. DePrince, S. K. Gray, X.-M. Lin and M. Pelton, *The Journal of Physical Chemistry Letters*, 2010, **1**, 2692-2698.
66. P. K. Sudeep, S. T. S. Joseph and K. G. Thomas, *Journal of the American Chemical Society*, 2005, **127**, 6516-6517.
67. H. Xiaoge, C. Wenlong, W. Tie, W. Erkang and D. Shaojun, *Nanotechnology*, 2005, **16**, 2164.
68. B. Hemmateenejad and M. R. Hormozi Nezhad, *The Journal of Physical Chemistry C*, 2008, **112**, 18321-18324.
69. B. Hemmateenejad, P. Shadabipour, T. Khosousi and M. Shamsipur, *Journal of Industrial and Engineering Chemistry*, 2015, **27**, 384-390.
70. M. R. Hormozi-Nezhad, Jalali-Heravi, M. and Kafrashi, F. , *J. Chemometrics,* , 2013, **27**, 353-358.
71. J. C. L. Sousa, M. G. Vivas, J. L. Ferrari, C. R. Mendonca and M. A. Schiavon, *RSC Advances*, 2014, **4**, 36024-36030.
72. B. Hemmateenejad, A. Safavi and F. Honarasa, *Chemometrics and Intelligent Laboratory Systems*, 2015, **141**, 88-93.
73. Y. Wang and Y. Ni, *Talanta*, 2014, **119**, 320-330.
74. K. Wongravee, T. Parnklang, P. Pienpinijtham, C. Lertvachirapaiboon, Y. Ozaki, C. Thammacharoen and S. Ekgasit, *Physical Chemistry Chemical Physics*, 2013, **15**, 4183-4189.
75. Y. Wang and Y. Ni, *Analyst*, 2014, **139**, 416-424.
76. Y. Kong, N. Zheng, Z. Zhang and R. Gao, *Journal of Chromatography B*, 2003, **795**, 9-15.
77. G. Chen, L. Zhang and J. Wang, *Talanta*, 2004, **64**, 1018-1023.
78. A. K. Sakhi, K. M. Russnes, S. Smeland, R. Blomhoff and T. E. Gundersen, *Journal of Chromatography A*, 2006, **1104**, 179-189.
79. S. K. Park, R. B. Boulton and A. C. Noble, *Food Chemistry*, 2000, **68**, 475-480.
80. W. Zhang, P. Li, Q. Geng, Y. Duan, M. Guo and Y. Cao, *Journal of Agricultural and Food Chemistry*, 2014, **62**, 5845-5852.
81. E. Hugo Seymour, S. J. Wilkins, N. S. Lawrence and R. G. Compton, *Analytical Letters*, 2002, **35**, 1387-1399.
82. L. Rover Jr, L. T. Kubota and N. F. Höehr, *Clinica Chimica Acta*, 2001, **308**, 55-67.
83. M. Hao, R. Liu, H. Zhang, Y. Li and M. Jing, *Spectrochimica Acta Part A: Molecular and Biomolecular Spectroscopy*, 2014, **125**, 7-11.
84. L. Ouyang, L. Zhu, J. Jiang and H. Tang, *Analytica Chimica Acta*, 2014, **816**, 41-49.
85. V. Sutariya, D. Wehrung and W. J. Geldenhuys, *Journal of Chromatographic Science*, 2012, **50**, 271-276.

Scheme 1.

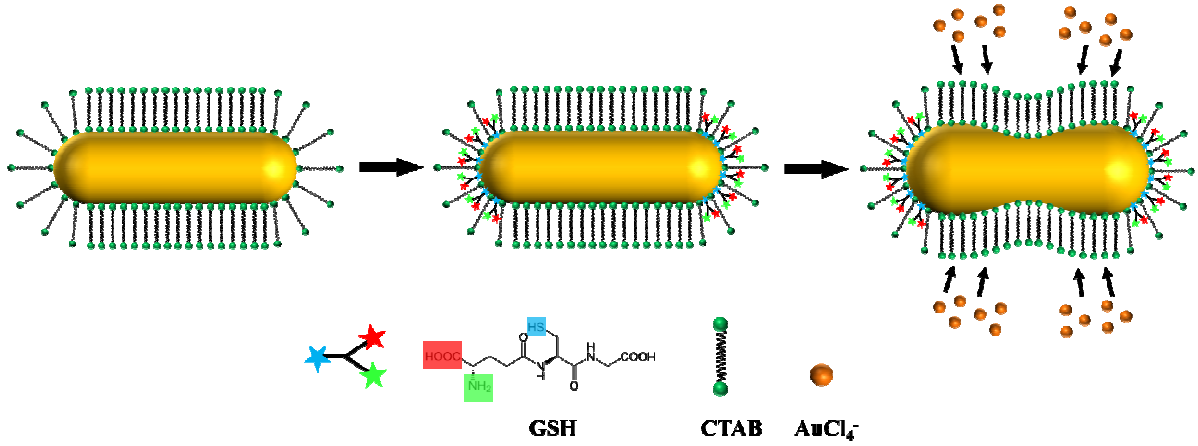

Scheme 1. Graphical illustration for transverse overgrowth on Au NRs induced by glutathione.

Figure 1.

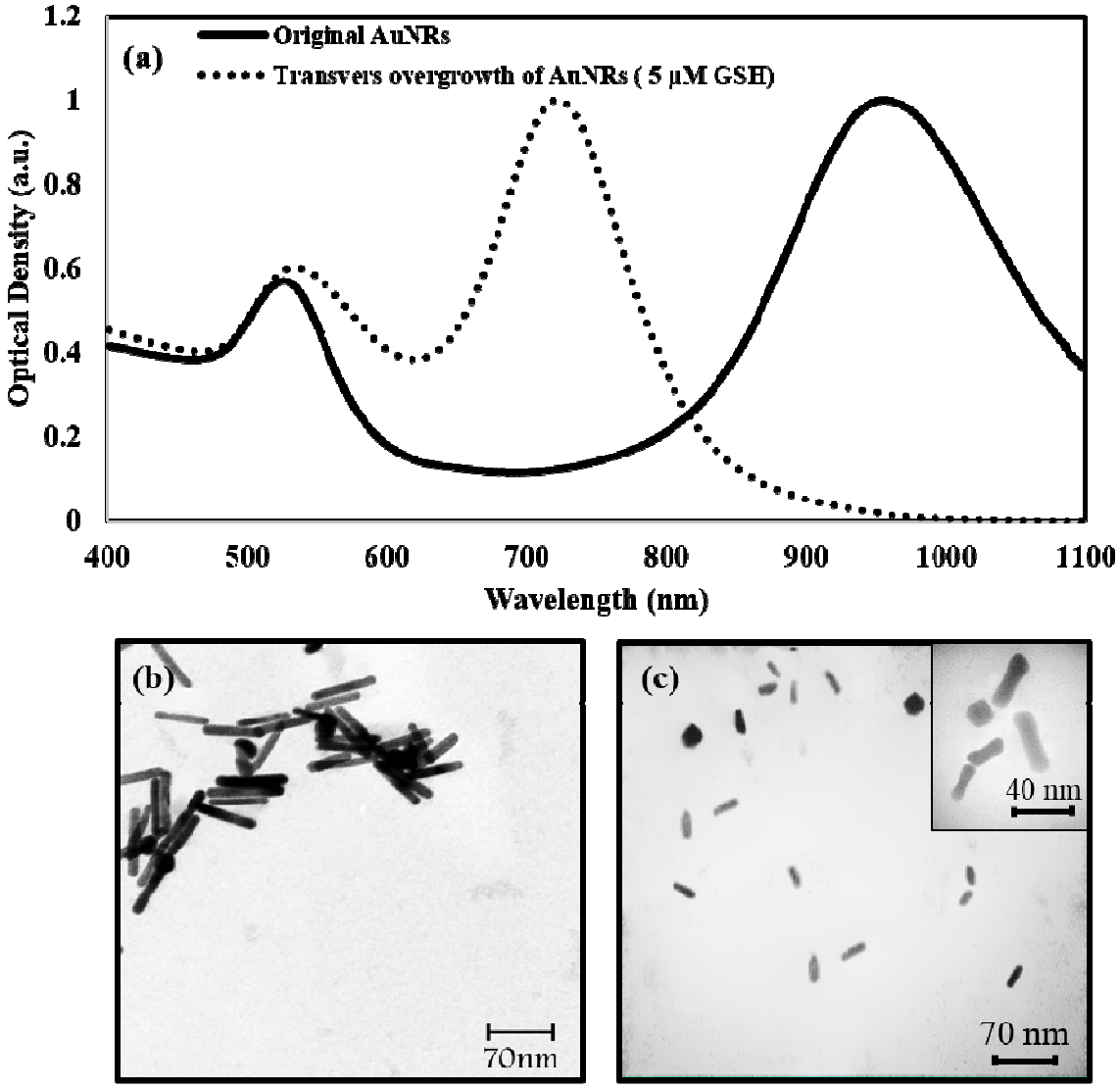

Figure 1. a) Normalized UV-Vis absorption spectra of the nanorods solution before and after growth process in presence of 5 µM GSH. b) TEM image of the original nanorods showing an aspect ratio of 6.5±0.2. c) TEM image of Au NRs after transverse overgrowth induced by 5 µM GSH.

Figure 2.

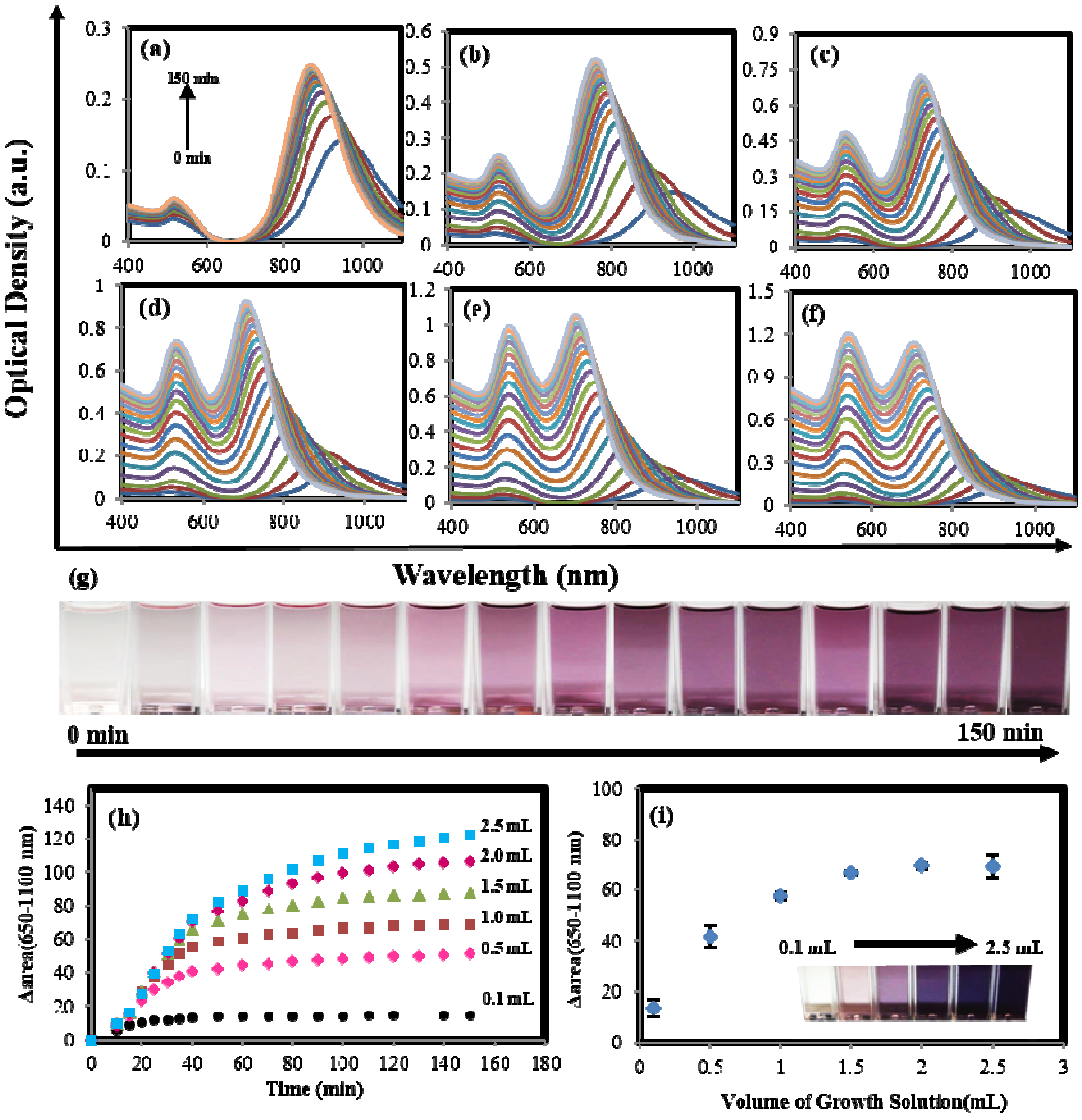

Figure 2. Variation of extinction spectra during transverse overgrowth on 1 mL of original Au NRs containing 5μM glutathione, upon addition of different volume of growth solution; a) 0.1 ml b) 0.5 ml c) 1 ml d) 1.5 ml e) 2 ml f) 2.5 ml of growth solution. g) Variation in color of solution during overgrowth process corresponds to d. (h-i) optimization of time for overgrowth process and volume of growth solution; The difference between surface area of the extinction spectrum at the range of 650nm to 1100 nm in absence and presence of growth solution was chosen as response and plotted versus a) reaction time for different volume of growth solution, and b) volume of growth solution. Inset in b is the color of solution for different volume of growth solution after the reaction completed.

Figure 3.

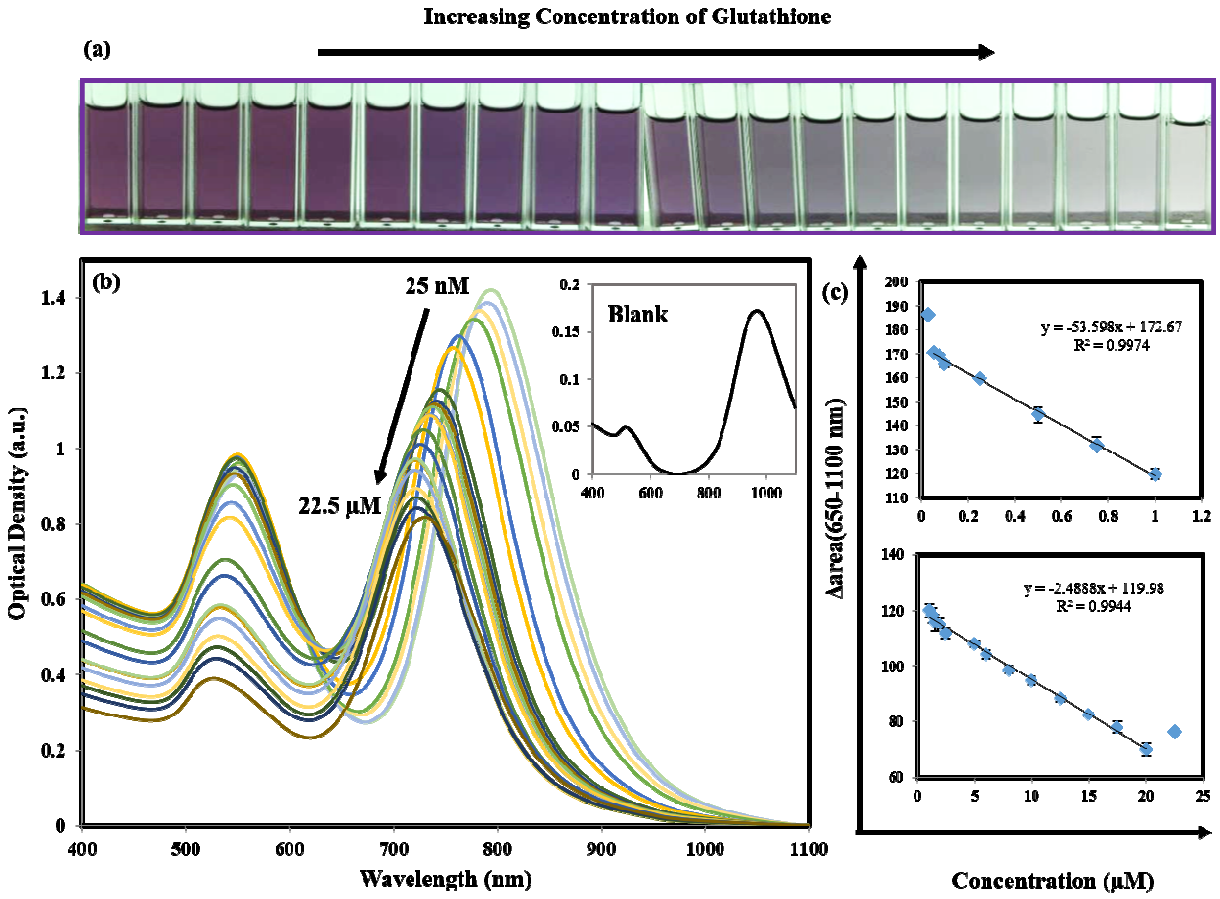

Figure 3. Colorimetric determination of GSH based on transverse overgrowth of NRs induced by varying concentration of GSH at optimum condition. a) Digital image of solutions at t=60 min according to increasing concentration of GSH. b) Extinction spectra of nanaorods solutions that contain different concentration of glutathione 60 min after initiation of overgrowth process resulted from addition of 1.5 ml growth solution to 1 ml of original NRs solution. c) Calculated calibration curve for determination of GSH showing two linear regimes at concentration ranges of 50 nM-1 µM and 1 µM-20 µM.

Figure 4.

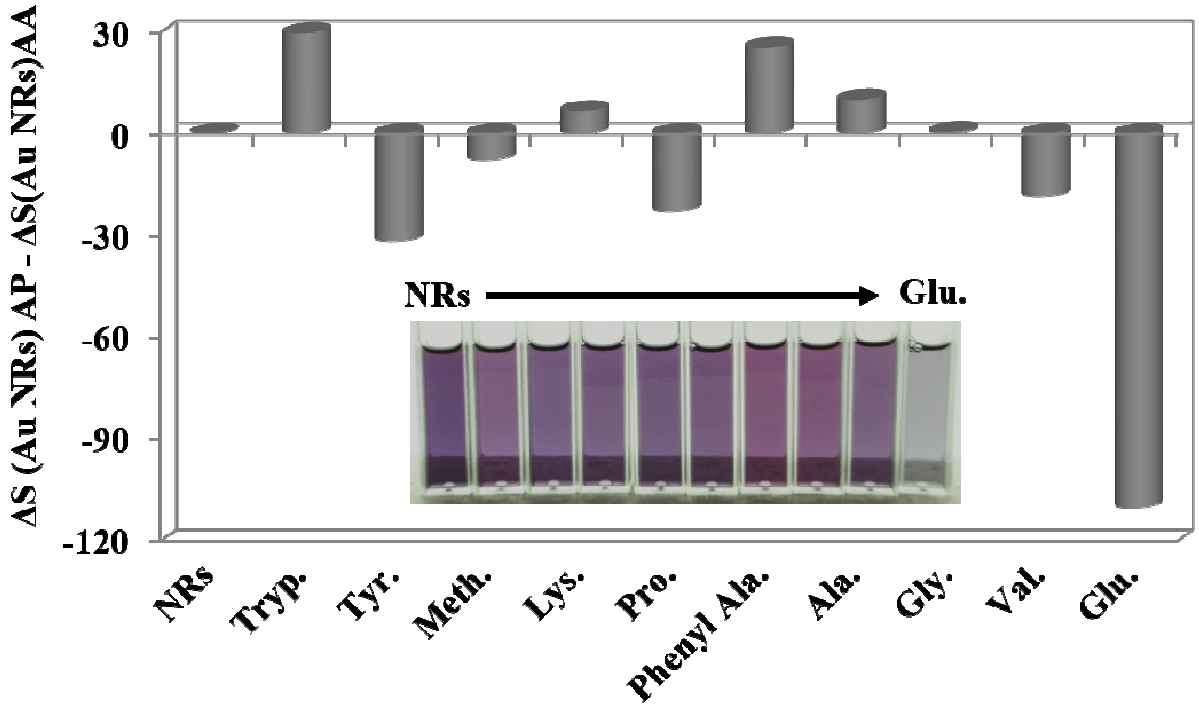

Figure 4. Selectivity assessment of the developed sensor for analyte-induced transverse overgrowth on Au NRs in compare to different amino acids. The concentration of GSH and other interfering species were 10 μM and 500 μM, respectively. Note for all cases, 1 ml aliquot of original nanorods solution and 1.5 ml of growth solution were utilized and the final volumes of solutions were adjusted at 3.6 ml.

Figure 5.

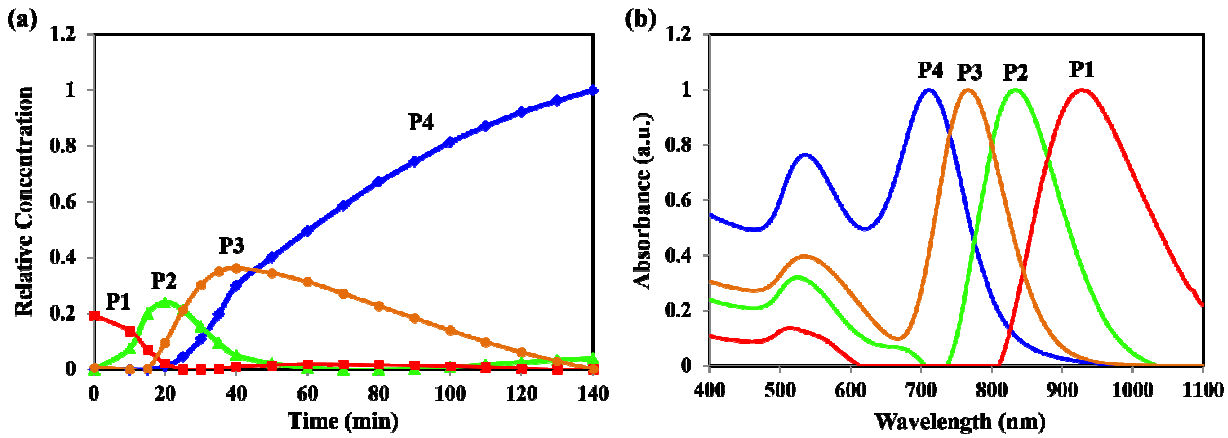

Figure 5. MCR-ALS analysis of four-factor system during transverse overgrowth on Au nanorods from addition of 1.5 mL of growth solution in presence of 5 μM glutathione. a) Normalized optimum concentration profiles and b) Calculated normalized pure spectra of the resolved particles. Component P1 is pristine nanorods (see scheme 1) and component P4 can be assigned to peanut-shaped nanoparticles according to our TEM analysis and findings of X. Kou et al [58].

Figure 6.

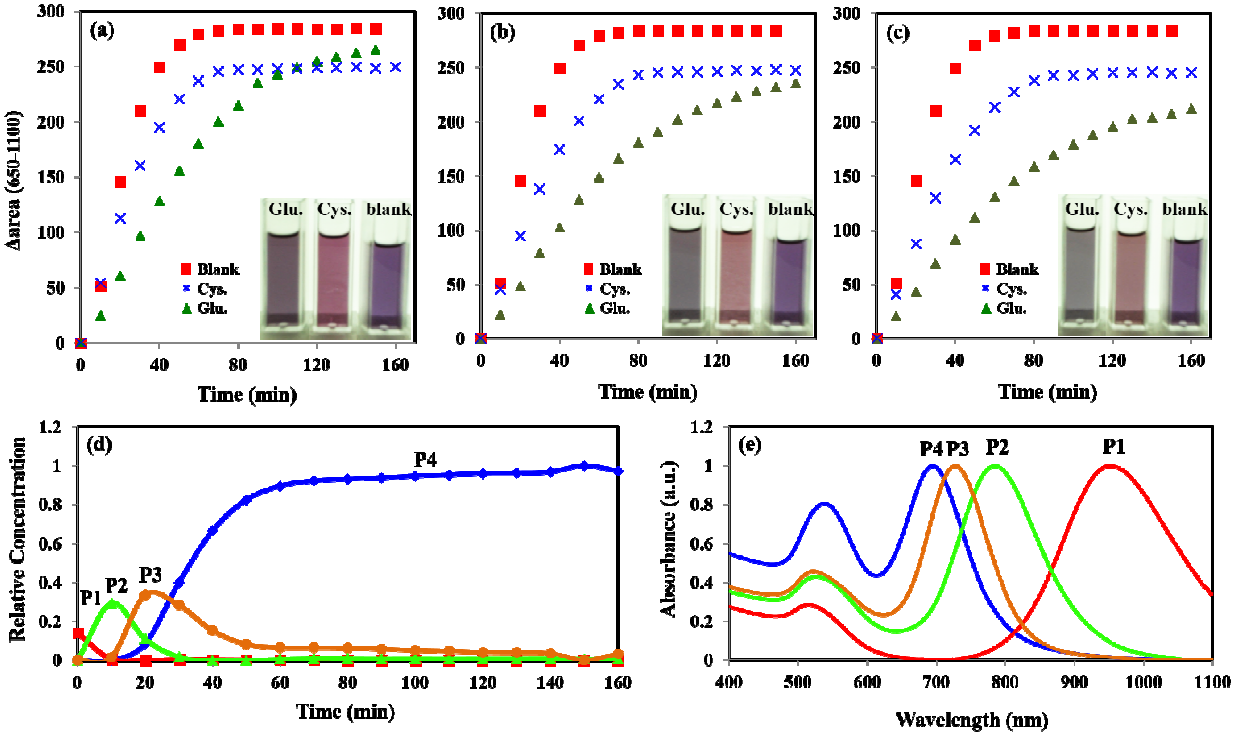

Figure 6. Comparison between kinetic of overgrowth on Au NRs induced by glutathione and cysteine having three different concentrations and in their absence (blank). a) 5 µM Glutathione, 5 µM Cysteine b) 10 µM Glutathione, 10 µM Cysteine c) 15 µM Glutathione, 15 µM Cysteine. Insets are digital images of produced nanoparticles solutions at corresponding concentration. Note for all cases, 1 ml aliquot of original nanorods solution and 1.5 ml of growth solution were utilized and the final volumes of solutions were adjusted at 3.6 ml. d) Normalized concentration profile and e) pure spectral profile obtained from MCR-ALS analysis on the recorded extinction spectra during overgrowth process induced by 1.5 mL of growth solution in presence of 5 µM micro of cysteine.

Table 1. Determination of GSH in plasma sample and complex mixture containing co-existing amino acids including Methionine, Alanine, Lysine, Glycine, Tryptophan, Tyrosine, Proline, Phenylalanine. The molar ratio of GSH to other species was 1:50.

Samples	Standard method (μM)	Added (μM)	Found (μM)	Recovery	RSD% (n=5)	Relative Error(%)
Amino acids mixture	-	5	5.27	105	1.74	-
	-	10	9.77	98	3.57	-
Plasma	0.485	0.5	0.53	106	6.64	3.00
	5.151	5	4.62	92	2.91	3.02
	9.653	10	10.41	104	4.96	4.47

Table 2. A comparison of the present method with literature for determination of GSH [*,]

Method/detector	Analytes/matrix	Label/Probe	LOD (μmol L^{1-})	RSD/%	Ref.
Colorimetric/UV-Vis	GSH/standards	none	0.04	1.9 (n=5)	This work
Colorimetric/UV-Vis	GSH/Trp, Tyr, Met, Lys, Pro, Phenyl Ala, Gly, Val [a]	none	-	1.74 for 5 μM GSH (n=5)	This work
Colorimetric/UV-Vis	GSH/Plasma	none	-	2.91 for 5 μM GSH (n=5)	This work
CE/ECD	GSH, GSSC/diabetic nephropathy (DN) patient's plasma	none	0.5 for standards and 6.30 for plasma sample	1.3 (n=6) for standards and 0.8 (n=3) for plasma	[76]
CE/ECD	GSH, Hcy, Cys, NAC/standards	none	2.9	-	[77]
HPLC/FD, ECD	GSH, GSSC/Human plasma	MBB	0.014	-	[78]
HPLC/FD	GSH, Cys, methanethiol, ethanethiol	OPA	0.033	-	[79]
HPLC/UV	GSH, Cys, Hcy, Cys-Gly	CNBF	0.06	< 3 (n=6)	[80]
Electrochemistry/CV	GSH/PBS	none	0.94	7.3 for 10 μM GSH (n=3)	[81]
Electrochemistry/AMP	GSH/serum [b]	none	19	-	[82]
FRET	GSH/Al^{3+}, Fe^{2+}, Mg^{2+}, Zn^{2+}, Ca^{2+}, Na^{+}, K^{+} [c]	RB	1	< 3 (n=3)	[14]
Fluorescence	GSH/THF:water (1:99, v/v) buffered at pH 7.2	AIE material	<1 [d]	-	[17]
Fluorescence	GSH: Cys with mole ratio 1:0.40	MMPB	3.23×10^{-4}	3.9 for 0.14 μM GSH (n=6)	[24]
MCE-LIF	GSH/mice hepatocytes in PBS	NDA	44.7	0.21	[83]
CL [e]	GSH/standards	Ce(IV)–quinine	5×10^{-4}	4.0 for 0.1 μM (n=11)	[19]
SERS (direct)	GSH/standards	none	0.05 [f]	-	[23]
SERS(dye probe)	GSH/standards	CV	0.04	7.1 for 0.5 μM (n=10)	[84]

[*] MBB (monobromobimane), OPA (o-phthalaldehyde), CNBF (4-chloro-3,5-dinitrobenzotrifluoride), MMPB (5-maleimidyl-2-(m-methylphenyl)benzoxazole), NDA (Naphthalenedicarboxaldehyde), RB (rhodamine B), CV (crystal violet).

[a] The molar ratio of GSH to other species was 1:50.
[b] Recovery percentages obtained with the biosensor for GSH (50 μM) solutions containing interfering compounds at 10.0 μM concentration showed significant interference from cysteine.
[c] The concentration of interfering species were kept at 0.1mM.
[d] The system reported to have a selective response to total of GSH and Cys in a matrix containing other aminothiols, including Cys, Gly, Ala, Leu, Val, Pro, Met, Phe, Trp, Ser, GSSC.
[e] The system reported to have a high selectivity for determination of 1.0 μM GSH in presence of Cys at molar ratio of Cys:GSH 1:1 and less.
[f] Simultaneous determination was not reported since the method was also very selective to Cysteine.